Neutron Veto Inefficiency Studies with FLUKA for the LDMX Hadronic Calorimeter

Jaida Raffelsberger
Project Supervisors: Einar Elén and Luis Sarmiento Pico
Project Duration: 2 months

Thesis presented for the degree of
Bachelor of Physics

LUNDS UNIVERSITET

Department of Physics
Division of Particle and Nuclear Physics
May 2023

Abstract

Dark matter accounts for about 85% of all matter in the Universe, yet its particle nature remains unknown [1]. The Light Dark Matter eXperiment (LDMX) is a proposed fixed-target missing-momentum experiment that intends to probe the predominantly experimentally uncharted MeV-GeV mass range for "light dark matter" (LDM) [2]. A significant challenge for LDMX is to efficiently veto rare photo-nuclear (PN) background events resulting in high energy ($\sim$3 GeV) neutral hadrons. The preliminary design of the sampling hadronic calorimeter (HCal), which is responsible for detecting neutral hadrons and consists of alternating layers of steel absorber plates and polystyrene scintillator bars, has been developed using GEANT4 simulations to realise the required veto inefficiency [3] [4] [5]. To validate the GEANT4 results, it was thus of interest and the aim of this project to perform a comparative study of neutron veto inefficiency between GEANT4 and other Monte Carlo codes, in this case FLUKA [6]. By modelling a simplified LDMX HCal geometry using the FLUKA Advanced InteRface (FLAIR) the neutron veto inefficiency as a function of HCal depth was found [7]. This was done for 0.1 GeV, 0.5 GeV, 1.0 GeV and 3.0 GeV incident neutrons with a threshold of 1 MeV and 10 MeV. Results indicate that FLUKA and GEANT4 are comparatively similar and independent of the thresholds. This indicates that the current design of the HCal with a depth of $\sim$3 m, is sufficient so as to ensure the veto performance for the relevant photo-nuclear backgrounds [2].

Popular Abstract

All matter we know and see only accounts for a mere 15% of all matter in the Universe [1]. The remaining 85% is known as "dark" matter since it does not interact electromagnetically and is thus invisible. Only indirect evidence for dark matter exists in the form of gravitational interactions with visible matter. By finding out what constitutes dark matter, insight into the fundamental structure and evolution of the Universe may be revealed.

One proposed experiment is the Light Dark Matter eXperiment (LDMX) that intends to probe for dark matter particles with low mass [2]. The LDMX aims to do this by directing high energy electrons on a fixed tungsten target, resulting in the electrons scattering off the target and in a rare process could produce dark matter particles. Since dark matter particles escape detection they are hence only quantifiable by the missing energy and momentum. However, it is more likely that Standard Model processes occur instead. It is therefore crucial for the LDMX to differentiate between processes that actually result in dark matter versus those that do not. Processes that do not result in dark matter then need to be efficiently vetoed by the detector. A key challenge for LDMX is to efficiently veto the process that results in single high energy neutrons.

Using simulations, the design of the sub-detector responsible for identifying neutrons has been optimised to a high degree of efficiency in order to veto single high energy neutrons. To ensure that the results acquired from previous simulations are accurate, it was of interest and the aim of this project to perform a comparative study using a competing simulation tool known as FLUKA [6].

This project found that there was little difference between the two simulation tools, and concludes that current LDMX sub-detector design considerations are likely to provide sufficient sensitivity and efficiency to veto single high energy neutrons.

Contents

List of Figures

List of Tables

List of Abbreviations

DM Dark Matter
LDMX Light Dark Matter eXperiment
LDM Light Dark Matter
PN Photo-Nuclear
EN Electro-Nuclear
ECal Electromagnetic Calorimeter
HCal Hadronic Calorimeter
EM ElectroMagnetic
SM Standard Model
WIMPs Weakly Interacting Massive Particles
SUSY SUperSYmmetry
MIPs Minimum-Ioninsing Particles
EoT Electrons on Target
SiPMs Silicon PhotoMultipliers
FLAIR FLuka Advanced InteRface

1 Introduction

Uncovering the particle nature of dark matter (DM) is at the forefront of modern particle physics, and may provide answers to fundamental questions about the creation of galaxies and galaxy clusters, as well as the structure and evolution of the Universe itself [2]. The Light Dark Matter eXperiment (LDMX) aims to probe the predominantly experimentally uncharted MeV-GeV mass range for "light dark matter" (LDM), including direct and via mediator particle production. It will also present sensitivity to dark sector physics, including strongly-interacting dark sectors, millicharges, axion-like and scalar particles [8].

The LDMX will confirm a dark matter signature by tagging an incoming beam electron on a fixed tungsten target, resulting in a low energy, moderate transverse-momentum recoil electron and the absence of a forward going photon or any final particle states [2]. The objective of the LDMX detector is thus to effectively conduct a high-statistics search for DM signal events and veto all standard model processes, particularly those that could imitate the signal-like signature, known as background events. Consequently, it consists of a tagging tracker for the incoming electron inside a dipole magnet, two trigger scintillator planes, a thin tungsten target, and a recoil tracker in the periphery of the magnetic field for the recoiling electron. An electromagnetic and a hadronic calorimeter (ECal and HCal) are primarily motivated by backgrounds with energetic photons, charged particles or neutral hadrons, which set the veto system requirements.

Most backgrounds are simple to reject due to large energy deposition in the ECal. A challenging and rare background for the HCal to veto is a final state of single $\sim$3 GeV energetic neutral hadrons, either neutrons or kaons. This background presents the basis of this project and motivates the design of the sampling HCal. The HCal requires sufficient sensitivity and low inefficiency such that no more than one in a million neutral hadrons go undetected.

Studies to optimise the HCal design were done internally by the LDMX collaboration and have found varying results using different versions of the detector simulation toolkit GEANT4 [3] [4] [5]. It is thus of interest to perform a comparative study to ensure that the proposed veto performance is sufficient, using competing radiation transport Monte Carlo simulation packages, in this case FLUKA [6]. The objective of this project will hence be to generate FLUKA samples of neutron veto inefficiency as a function of detector depth with a simplified LDMX sampling HCal geometry, and compare with the corresponding independent GEANT4 samples.

This work is organised as follows: Section 1 introduces this degree project and presents a broad overview including the project goal. Section 2 describes the theory underlying this study, including fundamentals about DM, the LDMX, neutron veto inefficiency, the HCal, and previous studies using GEANT4. Section 3 recounts the methodology used to achieve the goal of this project, including the simulation tool FLUKA and its graphical user interface FLAIR, as well as the data processing required to analyse the simulation data. Section 4 outlines the results of the project, while Section 5 discusses these results, as well as suggests improvements and possibilities for future studies. Section 6 concludes this project and summarises its significant findings.

2 Theory

2.1 Light Dark Matter

Non-baryonic matter accounts for about 85% of all matter in the universe and is believed to play a fundamental role in its structure and evolution, yet its particle nature remains unknown [1]. It is named "dark" matter as it does not interact electromagnetically and the only evidence for its existence is attributable to gravitational interaction with baryonic matter. These include gravitational lensing, galactic rotation curves, velocity dispersions, radiation galaxy clusters and cosmic microwave background radiation [9].

Regarding the origin of DM, one straightforward scenario is that it arose as a thermal relic from the hot early Universe due to small, non-gravitational interactions with Standard Model (SM) particles [2]. Thermal equilibrium between DM and SM matter and the residual relic abundance is achieved if the DM-SM interaction rate was once greater than the Hubble expansion rate. The observed relic abundance of DM particles at "freeze out" indicates a minimum annihilation rate of $\langle \sigma v \rangle \sim 10^{26} \mathrm{cm}^3 \mathrm{s}^{-1}$ [2]. This scenario, that DM is a thermal relic with a minimum annihilation rate, constrains the thermal mass range of DM particles from $\sim$MeV to $\sim$10 TeV, so it is comparable to SM matter.

The upper mass range from $\sim$GeV to $\sim$ TeV has been well explored in both direct and indirect detection experiments that are primarily motivated by the link between the dark matter particle candidate, known as Weakly Interacting Massive Particles (WIMPs), and supersymmetry (SUSY). Hitherto, these investigations have not been as conclusive as anticipated. The lower mass range from MeV to GeV, where most of the stable constituents of SM matter reside, has not yet been well examined. Sub-GeV DM has become a priority to investigate due to indications of DM being associated with a hypothetical "dark sector", comprising of a collection of new dark particles [10].

2.2 The Light Dark Matter eXperiment

The Light Dark Matter eXperiment is a proposed fixed-target missing momentum experiment that intends to probe direct and mediated DM creation in the sub-GeV mass range [2]. Beyond light thermal relics, LDMX is sensitive to non-thermal sub-GeV DM and other dark sector physics, including millicharges, axion and scalar particles, dark photons and other gauge bosons [8].

2.3 The LDMX Signal and Background Processes

LDMX aims to probe for DM by tagging and directing individual electrons from a low intensity, high luminosity electron beam on a thin tungsten target [2]. Potential DM production is seen in Figure 1, where a beam electron recoils and cedes most of its energy to invisible particles. In Figure 1a, a low energy and moderate transverse-momentum electron recoils on the nucleus, directly radiating a DM particle-antiparticle pair χ. In Figure 1b, in the target or calorimeter and depending on the mass of χ and mediator A', a dark photon decays into a DM pair or a DM pair is pair-produced by a virtual dark photon A'*. In Figure 1c, a photon produced in the target is converted to a vector meson V through photo-production in the calorimeter, which ultimately decays to a DM pair. The potential DM particles subsequently pass through the tracking planes and calorimeters invisibly, without interacting further, resulting in a missing energy and momentum signature.

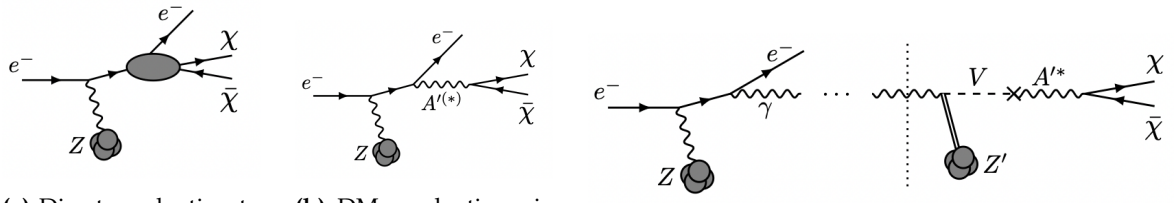

(a) Direct production to DM particle χ and its antiparticle $\bar{\chi}$.

(b) DM production via a dark photon mediator A′.

(c) DM production via a virtual dark photon A′* and a vector meson V.

Figure 1: Schematic depiction of DM production directly or via mediators. Taken from [11].

The potential DM signal consists of a recoil electron with an energy much less than that of the incident electron energy as shown in Figure 2a. The remainder of the signal would be a transverse momentum kick and no visible final state activity, as the missing energy and momentum is carried away by a dark photon that has escaped detection. LDMX must differentiate between the signal event and other SM processes. As shown in Figure 2b, backgrounds are other SM processes that imitate the signal, by the recoil electron energy being much less than the incident electron energy and undetected final state particles, resulting in a similar signature in the detector as the DM signature.

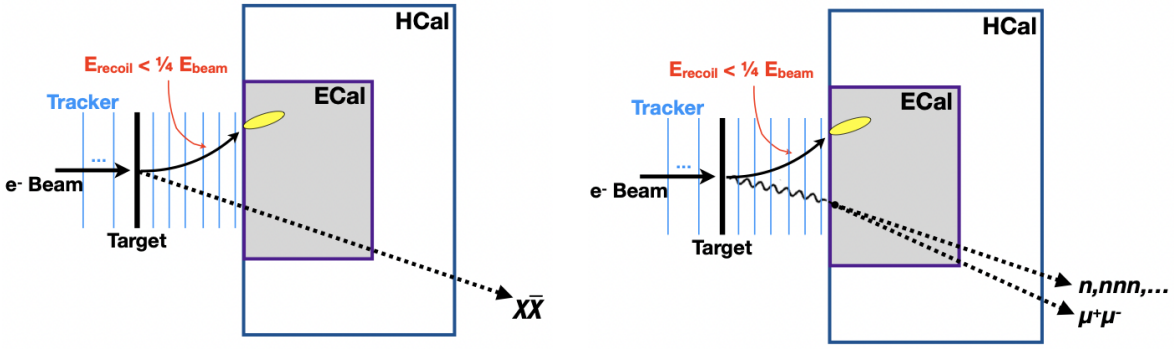

(a) LDMX detector schematic with a depiction of the signal process. An electron is directed towards the target, resulting in a recoil electron detected in the ECal and an undetected DM particle-antiparticle pair.

(b) LDMX detector schematic and a background process of hard bremsstrahlung in the target and a PN reaction in the ECal. The DM signal signature is imitated when most of the energy is carried away by undetected final states.

Figure 2: Layout of important LDMX detector components as well as depictions of the signal and possible background processes. Taken from [12].

Relevant backgrounds include low energy incident particles or beam impurities, leading to low energy electrons which mimic the signal recoil. As shown in Figure 3, the highest rate event is an incoming electron that does not interact in the target, and instead is distinguished from the signal by initiating a high energy ∼4 GeV shower in the ECal. The ECal may have a lower energy deposition due to potential PN or electro-nuclear (EN) interactions. Lower rate processes from electrons include EN reactions in the target and neutrino production.

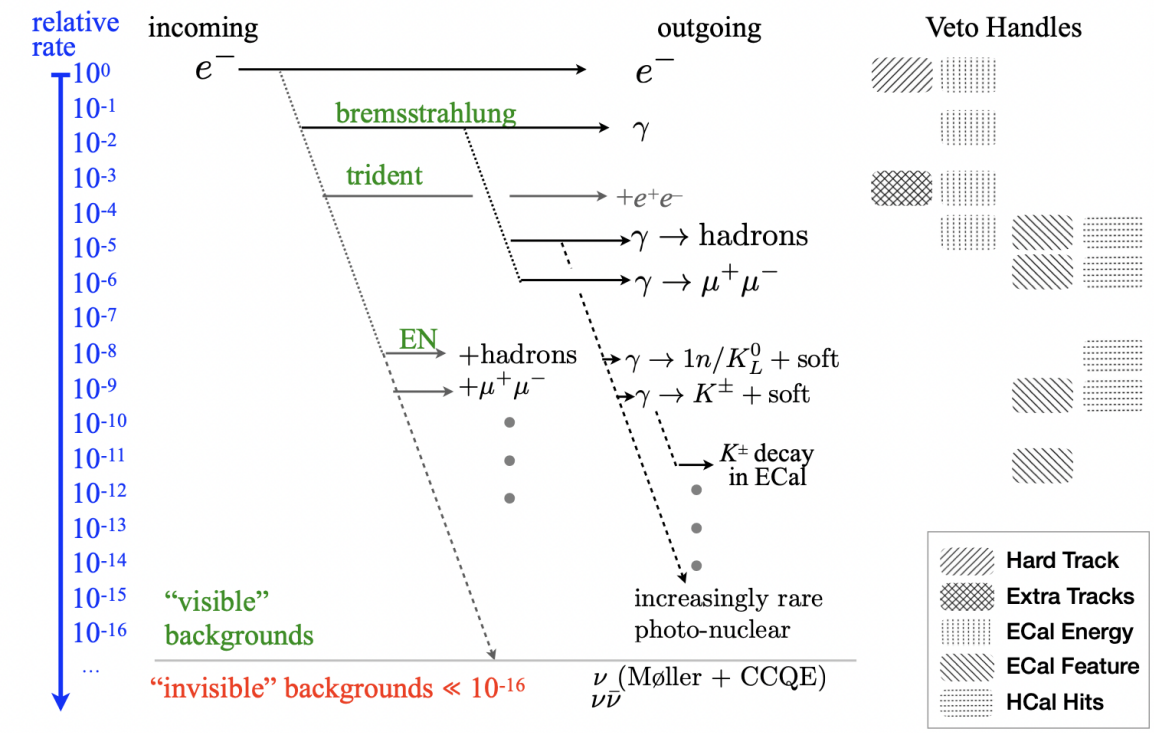

Figure 3: Veto design driving background processes for a 4 GeV electron beam energy. Veto handles refer to the corresponding detector systems for each background. Taken from [12].

The next set of background processes occur when the incoming electron undergoes bremsstrahlung in the target or the ECal, resulting in a recoil electron with only a small fraction of the incident beam energy, known as "hard" bremsstrahlung. The hard photon with the greater fraction of incident beam energy can then undergo conversion (pair production) and initiate an electromagnetic shower in the ECal or convert to muon or pion pairs for instance. A rare background occurs if the bremsstrahlung photon undergoes a photo-nuclear (PN) reaction in the target or ECal absorber creating hadrons. By then "escaping" the ECal, the photon energy is underestimated and imitates an invisible signal-like signature, making backgrounds with a small number of high energy particles as final states particularly important to veto. Such photon-induced backgrounds that result in minimum-ionising particles (MIPs) or charged and neutral hadrons require the complementary use of several veto handles. The rejection strategy for PN backgrounds includes ECal shower profile rejection (which varies from DM signals), hadronic tails from backwards charged hadrons or energetic forward neutral hadrons which relies on an efficient HCal, and finally tagging and recoil trackers for events that are not vetoed by either calorimeter.

The basis of this project is a PN background process where a hard photon transfers most of its energy to a single ~3 GeV final state neutral hadron. This is a particularly challenging background to veto due to its ability to fake a signal by surviving the regular, previous veto. Since a single high energy neutral hadron relies solely on the HCal to be detected, this background process thus determines the high veto efficiency, sensitivity and geometry (predominantly depth) of the HCal.

As shown above in Figure 3, PN events occur at a rate of ~2x10^{-5} per incident electron, while a

neutral hadronic final state has a rate of $\sim 10^{-3}$ per incident PN event. In Phase I of the experiment, LDMX is anticipated to direct a 4 GeV beam with $4x10^{14}$ electrons on target (EoT) [11]. Hence, one can expect $\sim 10^{6}$ events resulting in a recoil electron and a single hard forward neutron with little other activity in the ECal. The HCal, responsible for detecting neutral hadrons, thus requires an inefficiency of at least $\sim 10^{-6}$ in order to veto this background of neutral hadrons in the few-GeV range. In other words, less than one in a million neutrons are allowed to pass undetected through the detector. This inefficiency is not a stringent requirement for lower energy neutrons compared to a single high energy $\sim$3 GeV neutron. Low energy neutrons are typically produced in PN reactions in conjunction with other particles in all directions. This increases the chance of the other veto handles catching an event signature, not only the side and back HCal which vetoes all neutral hadrons. There is a greater chance that at least one of the numerous neutrons is vetoed, while the other liberated charged particles are detected by the ECal.

2.4 The LDMX Detector Concept

The objective of the LDMX detector, seen in Figure 4, is to effectively conduct a high-statistics search for DM signal events and reject background events. The signal process is detected by measuring the momentum of the incoming and recoiling electron, from which the mass and direction of DM can be deduced from the relative transverse momentum and the overall relative momentum, respectively. These measurements require a target and tagging tracker inside a dipole magnet, as seen in Figure 5. The tagging tracker focuses on incoming beam electrons with correct energy. The recoil tracker centres on low-momentum recoil electrons and collaborates with calorimeters to categorise signal and background events. The two trigger scintillator planes are needed to compile noteworthy events. The primary purpose of the calorimeters is to detect non-interacting electrons, bremsstrahlung photons and any other resulting particles. Charged particles will result in electromagnetic (EM) showers and are easily reconstructed in the ECal. It is more challenging for the ECal to reject when most of the bremsstrahlung photon energy is transfered to a few neutral hadrons in PN reactions with energies from 100 MeV to $\sim$3 GeV. Events resulting in a single high energy neutral hadron leave very little activity except for the recoil electron in the ECal. Therefore, the HCal is relied upon to exclusively detect single high energy neutral hadrons with very low inefficiency.

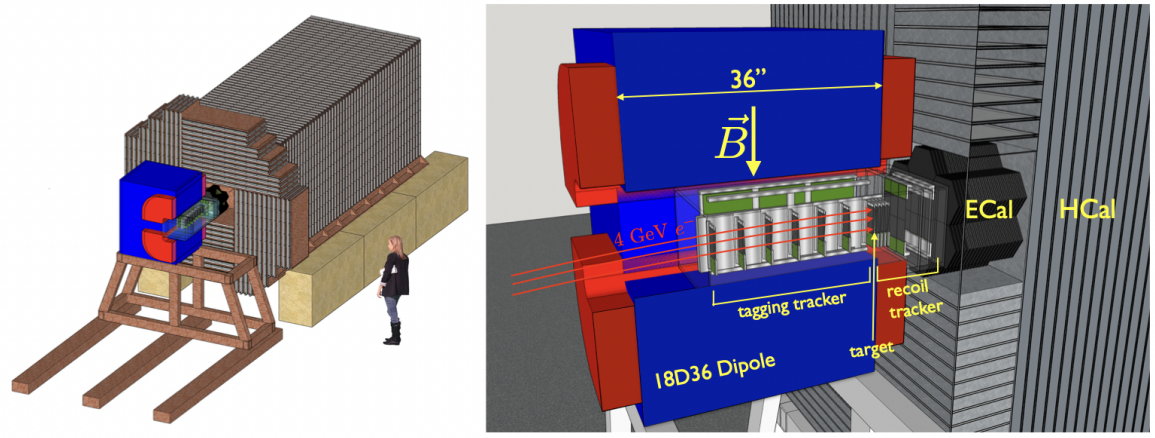

Figure 4: Depiction of the LDMX detector to the as well as a zoomed-in cutaway of the LDMX detector. Taken from [11].

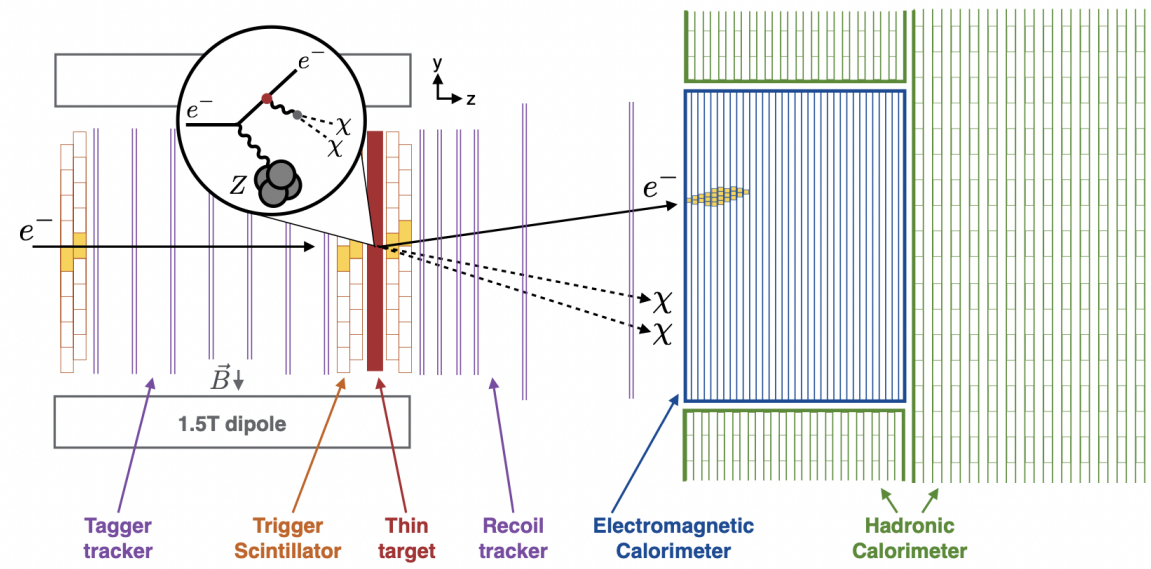

Figure 5: Schematic of the LDMX detector showing a possible production process of DM and the detector subsystems involved. The incoming electron is scattered on the target, resulting in DM and a recoil electron detected in the ECal. Taken from [11].

2.5 The Hadronic Calorimeter

A sampling HCal consists of layers of "passive" absorber material and "active" detector material [1, Ch. 4.4.6] [9, Ch. 4.7]. The absorber material is selected to have relatively high probability for particle collision, thus resulting in particle showers. This makes steel absorber plates an appropriate choice for the LDMX HCal [2]. When a high energy particle hits the absorbing material, multiple secondary particles are produced from the interaction with a fraction of the initial incoming energy. These in turn interact to produce a cascade or shower of particles until the lowest energy particles are completely stopped by the absorber.

The active material used is a scintillator detector, which in the LDMX consists of polystyrene scintillator bars [2]. In scintillator detectors, ionising particles excite molecules which de-excite to emit scintillation photons typically in the visible or UV region [13, Ch. 7] [9, Ch. 4.4.2]. Dopants in the scintillator ensure that the scintillator light is reabsorbed by flouresent molecules, which quickly emit longer-wavelength photons via radiative decay. Silicon photomultipliers (SiPM) are coupled to the scintillators via wavelength-shifting fibers and convert the photons into an electrical signal [2].

The design of the HCal is mainly motivated by the need to veto low energy moderate-angle neutron pairs which drive the back HCal width [2]. A side HCal is used to detect neutral hadrons travelling at large polar angles. High energy single neutrons mostly travel forward due to energy conservation and thus drive the depth of the detector. A deeper detector implies a lower chance of the neutron passing through without reacting. The rate at which the inefficiency decreases with depth is dependent on the absorber thickness. A thicker absorber will result in a faster decrease in inefficiency. However, a layer that is too thick may stop the neutrons completely before they reach the scintillator layer. Moreover, the cost of detector materials and space availability are also significant motivators for HCal optimisation.

2.6 Detector Simulation

Simulations are crucial to designing and analysing an experiment. Monte Carlo simulations model the probability of different outcomes that are difficult to predict due to stochastic variables. An uncertain variable is appointed multiple inputs and by averaging over the multiple outputs an estimate is achieved. Monte Carlo radiation transport codes are computational algorithms specifically used for simulating radiation-matter interactions. Both the detector apparatus can be modelled and the general physics processes simulated which remain detector independent [9, Ch. 8.4.3]. They rely on random sampling to produce events and treat one particle, one step at a time.

3 Methodology

3.1 Project Goal

The purpose of this project was to determine neutron veto inefficiency as a function of detector depth for 0.1 GeV, 0.5 GeV, 1.0 GeV and 3.0 GeV incident neutrons with thresholds of 1 MeV and 10 MeV, with a simplified geometry of the LDMX sampling hadronic calorimeter. To produce a sample of Monte Carlo events, the simulation tool FLUKA was used, and allowed for comparison with the competing detector simulation tool GEANT4.

3.2 FLUKA and GEANT4

The Monte Carlo code used in this project is known as FLUKA, specifically version 4-3.1, and has significant applications in high energy experimental physics such as accelerator design, medical physics, engineering as well as detector simulation and shielding [6]. FLUKA can simulate in any material the interactions and transport of photons, hadrons and leptons from few keV to high cosmic-ray energies. To be able to manipulate FLUKA code to suit the problem of this project, the advanced graphical user interface known as Fluka Advanced InteRface (FLAIR) version 3.2-1 was used [7].

The GEANT4 toolkit is the Monte Carlo code used in previous simulation studies by LDMX to guide detector design [3] [4] [5]. The LDMX collaboration used a C++ event processing and simulation framework called ldmx-sw, which uses the FTFP_BERT physics list but with changes to the Bertini Cascade for PN reactions. The results displayed in [2] are not directly comparable since the HCal veto is defined differently in terms of energy deposition per scintillator bar, with energy in terms of photoelectrons. Moreover, the polystyrene scintillator and steel absorber thickness was 20 mm and between 2-100 mm, respectively. In this study, comparable GEANT4 samples had to be generated using the GEANT4 version 10.2.3 with LDMX-specific modifications (version 4). These samples had a simplified LDMX HCal geometry with no air gaps between the steel absorber and polystyrene scintillators, as well as the same number and width of layers as the FLUKA samples. It also did not take into account Birks law, which refers to the light output of organic scintillators per unit length. Ideally, the emitted fluorescent light is linearly proportional to the energy deposition of the ionising particle, but deviations arise due to the quenching effects of excited particles [13].

3.3 Experimental Setup as Simulated in FLUKA

The experiment was set up using the input window of FLAIR, as seen in Figure 13 in Appendix A. A more detailed description of the experimental setup is also found in there. The neutron beam energy was set to first to 0.1 GeV, 0.5 GeV, 1.0 GeV and then 3.0 GeV. This energy range was informed by previous results seen in [2]. The greater energies allow for analysis of the veto inefficiency of a single

high energy neutron and allow for the estimation of the depth of the back HCal. The lower energies were chosen to study the behaviour of PN reactions resulting in numerous lower energy neutrons. This is of particular significance for the side HCal design, where most of the lower energy neutrons are detected. Moreover, scrutinising the performance of FLUKA compared to GEANT4 for lower energy neutrons may benchmark the accuracy of any higher energy results.

A description of the HCal geometry was modelled. As seen in Figure 6a, it consists of 192 layers of alternating absorber plates and scintillator bars (with no air gaps), both with 2 cm thickness so that the total detector has the dimensions of 200 cm x 200 cm x 384 cm. The thickness for both layers was chosen to be the same to simplify later analysis and is the main difference to the LDMX HCal. However, since the principle goal of this project is to establish any differences between two simulation tools, a more detailed geometry will have negligible effects on result authenticity since the generated GEANT4 samples used also have a simplified geometry. The materials stainless steel and polystyrene were assigned to the absorber and the scintialltor region, respectively, as seen in Figure 6b.

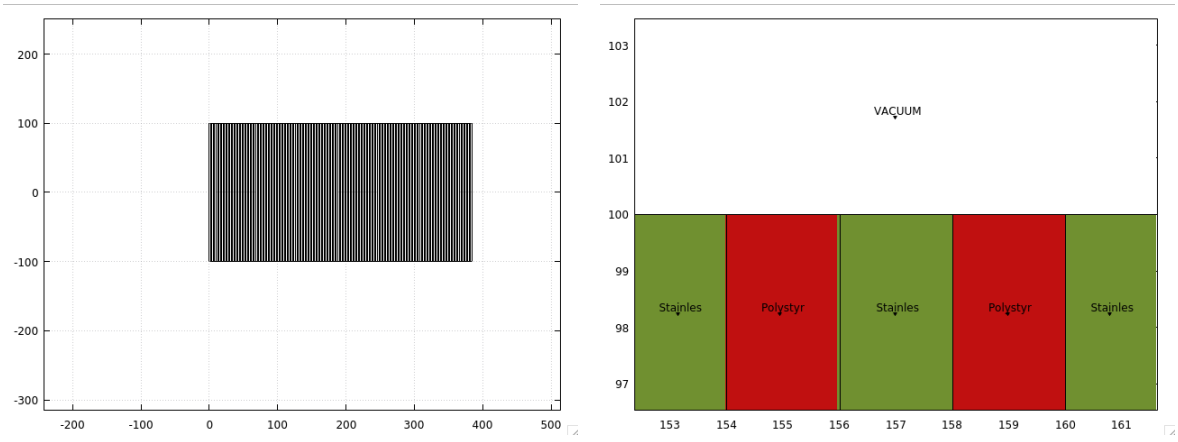

(a) Geometry of the simplified HCal used in this project showing 192 layers each of dimensions 200 cm x200 cm x 2 cm.

(b) A zoomed-in figure of the geometry of the simplified HCal showing the 2 cm layers of stainless steel and polystyrene.

Figure 6: Geometry of the simplified HCal as displayed in FLAIR.

The Eventbin estimator was used, which reproduces data with an energy deposition after each event, one event at a time. One event signifies one neutron directed to the HCal. The binning structure was set to 1x1x192, meaning that there are 192 bins in the z-direction, and one bin in the x- and y-directions. This allowed for an ASCII file of one energy deposition result in every steel and polystyrene layer for every event.

3.4 Data Processing

After running the simulation, code was used to parse and analyse the data in the ASCII files. This is seen in the Appendix B. Histograms describing total energy absorbed and greatest energy deposition were created using 100000 events as proof of concept and development. Inefficiency was then defined as counts of undetected neutrons, divided by the total number of events, which was set to 10 million. 10 million was used so as to allow prediction of detector depth at an inefficiency of one in a million.

This resulted in histograms of inefficiency as a function of detector depth. Uncertainties were taken into account, with error bars set to the square root of the normalised inefficiency value. "Normalised" referring to counts of undetected neutrons divided by the total number of neutrons. Figures of the ratio of the FLUKA histogram with respect to the GEANT4 histogram,

$$\frac{\text{Counts of FLUKA Inefficiency}}{\text{Counts of GEANT4 Inefficiency}}, \tag{1}$$

as well as the relative difference,

$$\frac{\text{Counts of FLUKA Inefficiency - Counts of GEANT4 Inefficiency}}{\text{Counts of GEANT4 Inefficiency}}, \tag{2}$$

were created to highlight the differences between the two simulations. Significant differences were displayed in tables, including the extremes of the ratio and relative difference and at which depth this occurred at, as well as the minimum inefficiency reached at a certain depth. The systematic uncertainty for the depth was taken as half the width of one layer.

Neutrons were deemed as undetected if they were only absorbed in steel absorber layers or below a threshold energy of either 1 MeV or 10 MeV in the scintillator layer. The veto used by [2] was defined in terms of photoelectrons per scintillator bar, while this study looked at the energy deposition in an entire layer. The question of different thresholds for LDMX is important as lower thresholds will trigger often, while higher thresholds inevitably neglect neutrons, but result in less experimental dead time which is due to significant noise accumulated in the entire detector from each detector channel. The range of threshold values was informed by the average energy deposited in each layer, while the particular values were chosen less rigorously, as the primary interest was in the difference between FLUKA and GEANT4 samples. Investigating two thresholds allowed for insight into the sensitivity of the inefficiency to the threshold, and if divergent neutron incident energies are relevant.

4 Results

4.1 Total Energy Absorbed in Steel and Scintillator Layers

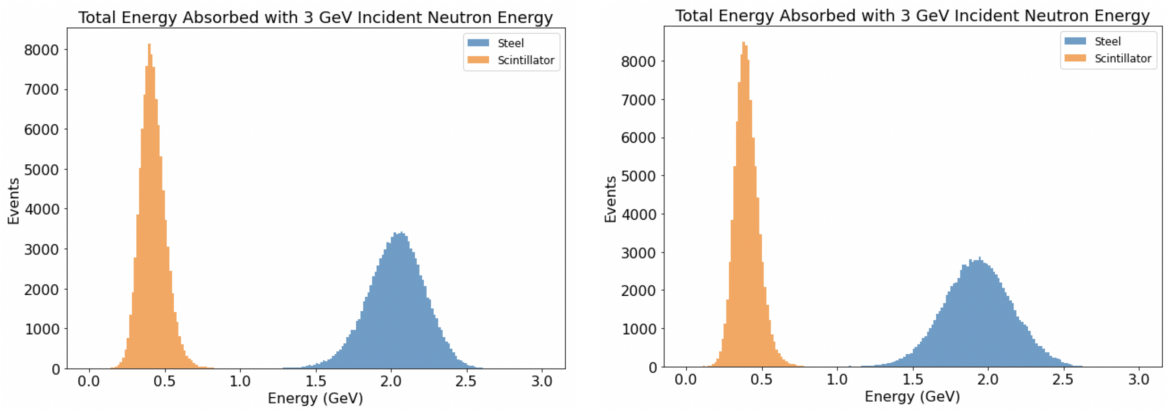

(a) FLUKA sample.

(b) GEANT4 sample.

Figure 7: Total energy absorbed in the steel and scintillator layers for 3.0 GeV incident neutrons.

Looking at Figure 7, for the polystyrene scintillator layer, the main difference between FLUKA and GEANT4 is that GEANT4 produces a slightly narrower distribution, thus reaching a greater number of events compared to FLUKA even as both distributions are centred at ∼0.5 GeV. For the steel absorber layer, the GEANT4 distribution is less narrow. It is more spread out over the energy range ∼1.5 GeV to ∼2.5 GeV compared to FLUKA and reaches a lower maximum number of events.

4.2 Position of Greatest Energy Deposition

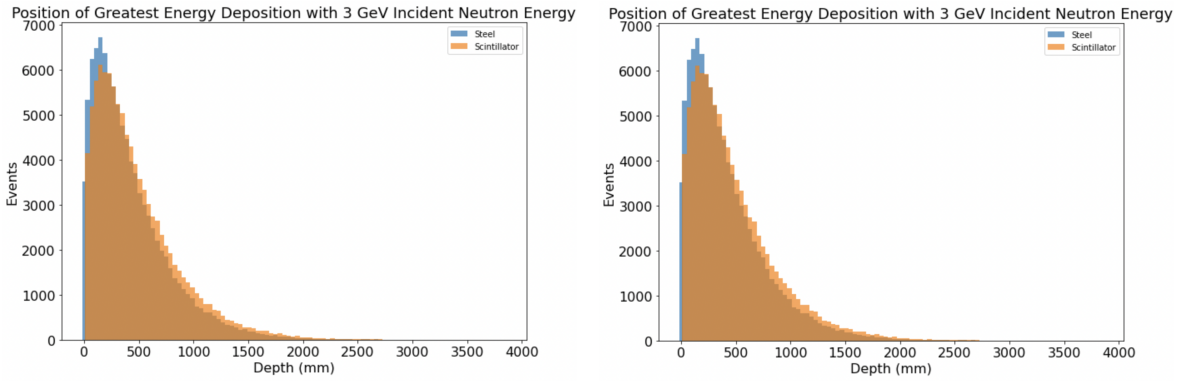

(a) FLUKA sample.

(b) GEANT4 sample.

Figure 8: Position of greatest energy deposition in the steel and scintillator layers for 3.0 GeV incident neutrons.

As seen in Figure 8, as a neutron is directed to the detector, most of the energy is initially deposited in the steel layers. Figure 8b, shows that GEANT4 has a distribution reaching a greater number of maximum events, compared to FLUKA in Figure 8a, which declines less steeply and has faintly more events at greater depths. Specifically looking at the scintillator layers, the first and maximum number of events occurs at the same depths for both simulations, while the last event for FLUKA occurs at a depth of 3830 mm and for GEANT4 at 3790 mm.

4.3 Single Neutron Veto Inefficiency

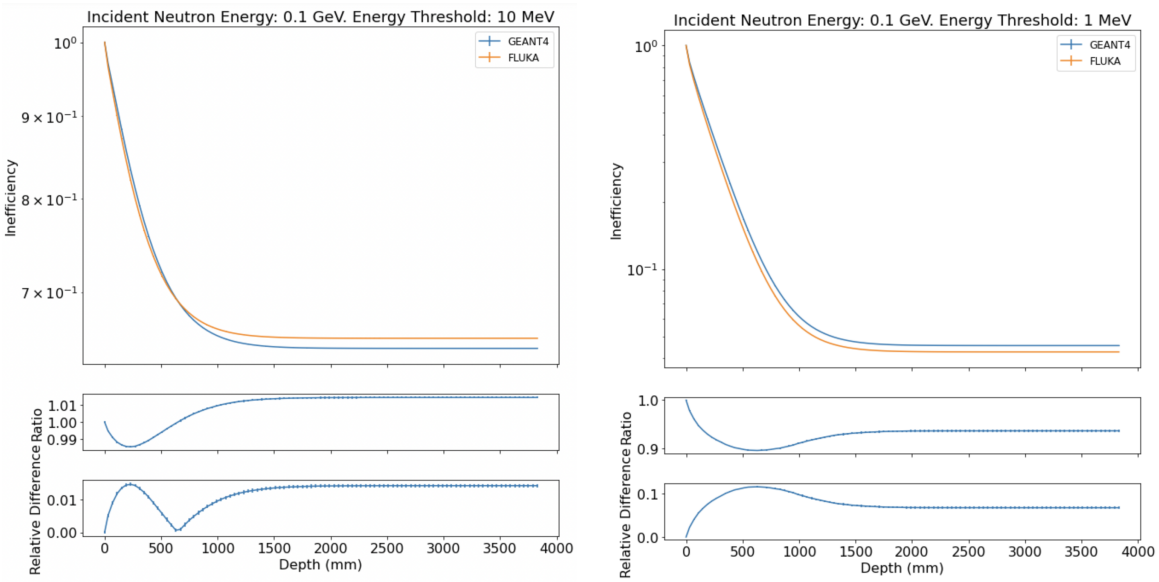

(a) Threshold of 10 MeV.

(b) Threshold of 1 MeV.

Figure 9: Single neutron veto inefficiency as a function of HCal depth for 0.1 GeV incident neutrons from FLUKA and GEANT4.

Energy Threshold	10 MeV		1 MeV	
Simulation Tool	FLUKA	GEANT4	FLUKA	GEANT4
Inefficiency	0.65522±0.00026	0.64582±0.00025	0.04258±0.00007	0.04546±0.00007
Inefficiency Depth (mm)	2670±10	2710±10	2670±10	2710±10
Ratio	1.0146±0.0006		0.8962±0.0012	
Ratio Depth (mm)	2470±10		630±10	
Relative Difference	0.0147±0.0005		0.1159±0.0015	
Relative Difference Depth (mm)	230±10		630±10	

Table 1: Differences between FLUKA and GEANT4 from Figure 9, showing the minimum single neutron veto inefficiency with its corresponding depth and the extrema of the ratio and relative difference with their corresponding depths.

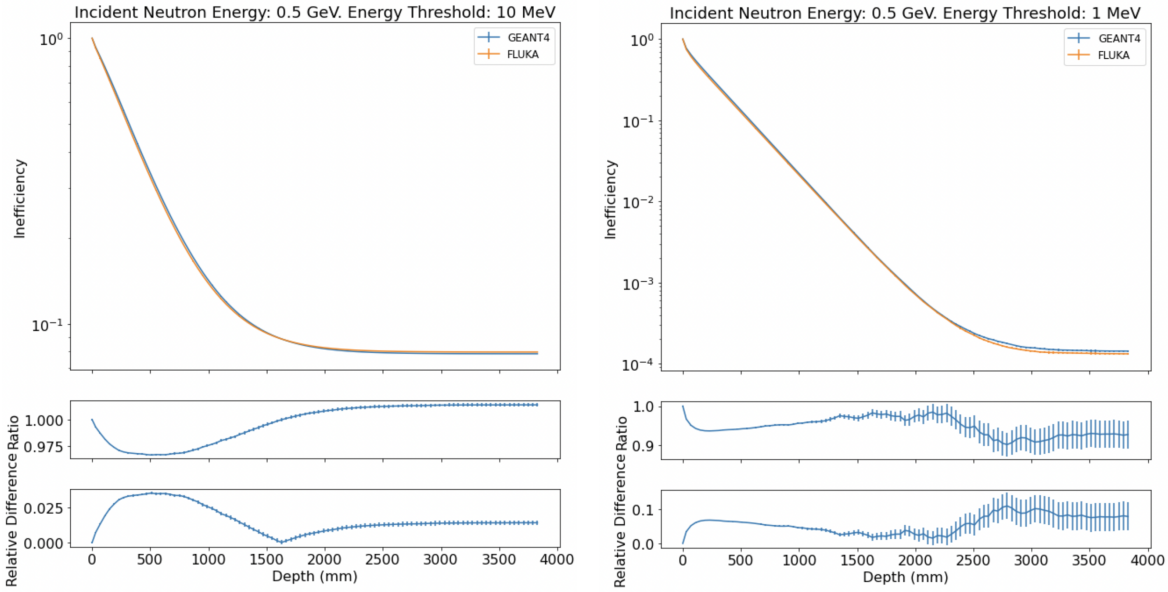

(a) Threshold of 10 MeV.

(b) Threshold of 1 MeV.

Figure 10: Single neutron veto inefficiency as a function of HCal depth for 0.5 GeV incident neutrons from FLUKA and GEANT4.

Energy Threshold	10 MeV		1 MeV	
Simulation Tool	FLUKA	GEANT4	FLUKA	GEANT4
Inefficiency	0.07977±0.00009	0.07865±0.00009	0.000133±0.000004	0.000143±0.000004
Inefficiency Depth (mm)	3830±10	3830±10	3630±10	3670±10
Ratio	0.9664±0.0008		0.901±0.031	
Ratio Depth (mm)	590±10		2790±10	
Relative Difference	0.0351±0.0008		0.11±0.04	
Relative Difference Depth (mm)	510±10		2750±10	

Table 2: Neutron veto inefficiency between FLUKA and GEANT4 from Figure 10, showing the minimum single neutron veto inefficiency with its corresponding depth, and then the extrema of the ratio and relative difference with their corresponding depths.

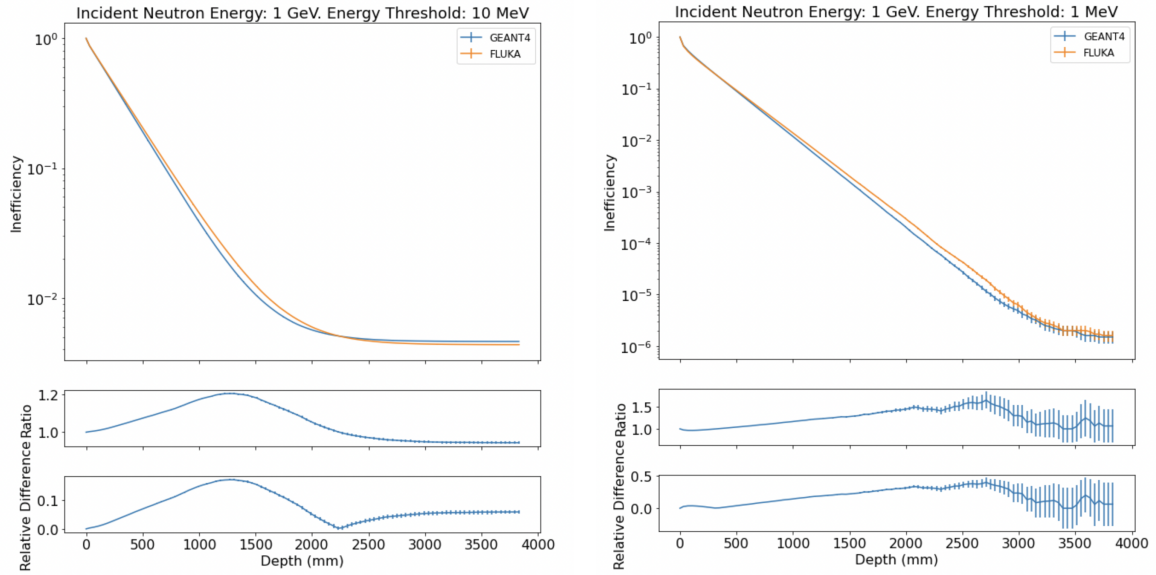

(a) Threshold of 10 MeV.

(b) Threshold of 1 MeV.

Figure 11: Single neutron veto inefficiency as a function of HCal depth for 1.0 GeV incident neutrons from FLUKA and GEANT4.

Energy Threshold	10 MeV		1 MeV	
Simulation Tool	FLUKA	GEANT4	FLUKA	GEANT4
Inefficiency	0.004360±0.000021	0.004614±0.000021	(1.6±0.4)x10^{-6}	(1.5±0.4)x10^{-6}
Inefficiency Depth (mm)	3750±10	3790±10	3830±10	3830±10
Ratio	1.204±0.004		1.66±0.20	
Ratio Depth (mm)	1270±10		2710±10	
Relative Difference	0.1691±0.0027		0.40±0.07	
Relative Difference Depth (mm)	1270±10		2710±10	

Table 3: Differences between FLUKA and GEANT4 from Figure 11, showing the minimum single neutron veto inefficiency with its corresponding depth, and then the extrema of the ratio and relative difference with their corresponding depths

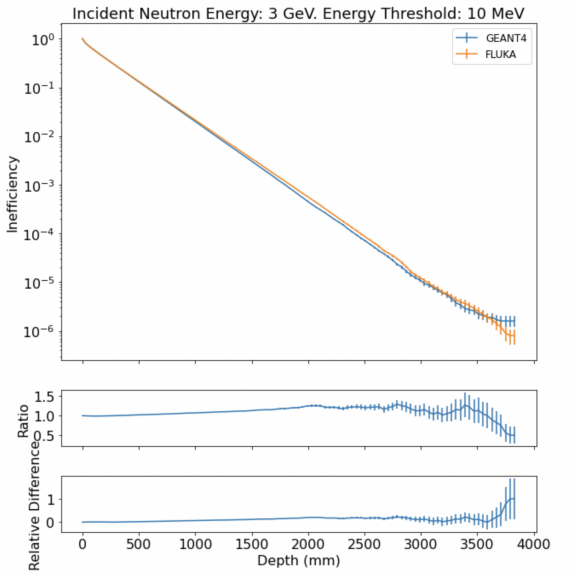

(a) Threshold of 10 MeV.

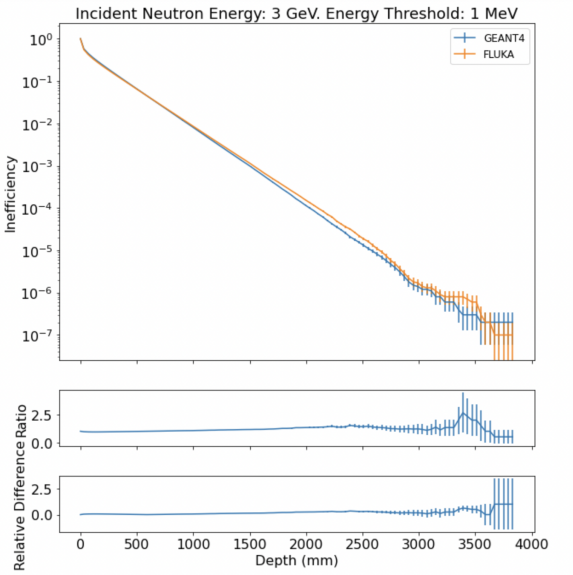

(b) Threshold of 10 MeV.

Figure 12: Single neutron veto inefficiency as a function of HCal depth for 3.0 GeV incident neutrons from FLUKA and GEANT4.

Energy Threshold	10 MeV		1 MeV	
Simulation Tool	FLUKA	GEANT4	FLUKA	GEANT4
Inefficiency	$(1.20\pm0.35)\text{x}10^{-6}$	$(1.6\pm0.4)\text{x}10^{-6}$	$(1.10\pm0.33)\text{x}10^{-6}$	$(1.10\pm0.33)\text{x}10^{-6}$
Inefficiency Depth (mm)	3710 ± 10	3830 ± 10	3150 ± 10	3110 ± 10
Ratio	1.30 ± 0.11		2.7 ± 1.8	
Ratio Depth (mm)	2790 ± 10		3390 ± 10	
Relative Difference	1.0 ± 0.9		1.0 ± 2.4	
Relative Difference Depth (mm)	3790 ± 10		3670 ± 10	

Table 4: Differences between FLUKA and GEANT4 from Figure 12, showing the minimum single neutron veto inefficiency with its corresponding depth, and then the extrema of the ratio and relative difference with their corresponding depths

5 Discussion

5.1 Total Energy and Position of Greatest Energy Deposition

The interactions of neutrons in the HCal was first studied by analysing plots of total energy absorbed in the steel absorber and polystyrene scintillator layers as well as the position of greatest energy deposition. This allowed some prediction into how significant the differences between the two simulation tools would be for the inefficiency studies. As seen in Figures 7 and 8, there is some but no meaningful distinction between FLUKA and GEANT4. However, the slight differences seen in Figures 7 and 8, can perhaps be attributed to how FLUKA and GEANT4 take into account neutron cross sections.

5.2 Single Neutron Veto Inefficiency

On the whole, there is no considerable difference between the single neutron veto inefficiency samples produced by FLUKA and those by GEANT4, and the inefficiency is insensitive to the choice of threshold for the neutron energy range studied.

In Figures 9-10 using 0.1 GeV and 0.5 GeV incident neutrons, FLUKA is mostly seen to predict a slightly smaller inefficiency than GEANT4, as highlighted in the corresponding ratio figures being less than 1, with the exception of Figure 9a for 0.1 GeV neutrons and 10 MeV threshold. The variation of FLUKA to GEANT4 reaches a minimum ratio of 0.8962 ± 0012, as seen in Figure 9b, for 0.1 GeV incident neutrons and a threshold of 1 MeV.

Figures 9-10 all result in plateaus before reaching the required inefficiency of 10^{-6}. The plateau occurs because low energy particles are completely absorbed by the steel layers and do not reach the scintillators. As mentioned, study of Figures 9-10 are more important for the side HCal, since neutrons of lower energy travel at large polar angles and are more likely detected by the side HCal.

In Figure 9 with 0.1 GeV incident neutrons and a threshold of 10 MeV, a minimum inefficiency of 0.65522 ± 00026 is reached, while at the same depth of 2670 ± 10 mm and a lower threshold of 1 MeV an inefficiency of 0.04258 ± 00007 is achieved. The values specified were produced by FLUKA, yet are within the same order of magnitude as those produced by GEANT4 as seen in Table 1. The differences become more prominent at greater depths.

In Figure 10 with 0.5 GeV incident neutron energy and 10 MeV threshold, a minimum inefficiency of 0.07977 ± 0.00009 is reached, while at a lower threshold of 1 MeV an inefficiency of 0.000133 ± 0.000004 is achieved. Unlike for 0.1 GeV neutrons, the plateau does not occur at the same detector depths for the two thresholds. The values specified were produced by FLUKA, but as seen in Table 2 the GEANT4 values are all within the same order of magnitude with differences even smaller than those seen for 0.1 GeV. Figures 9-10 show that for a threshold decreasing by one order of magnitude, a lower inefficiency is achieved, while an increasing incident neutron energy also decreases the inefficiency achieved. This is made clearer by Figure 15 in Appendix C, which plots the minimum inefficiency achieved by the FLUKA samples.

The aforementioned lower energies 0f 0.1 GeV to 0.5 GeV are of central importance to the side HCal design, which is situated around the main HCal so as to catch numerous lower energy neutral hadrons travelling at large polar angles. Reaching the strict inefficiency 10^{-6} is not essential, nevertheless the figures of inefficiency provide insight into the differences between the two simulation tools FLUKA and GEANT4 as a whole. These results may also provide a basis for future study to confirm or improve the side HCal and the veto requirements for lower energy neutral hadrons.

In Figures 11-12 with 1.0 GeV and 3.0 GeV incident neutrons, FLUKA is mostly seen to predict a slightly greater inefficiency than GEANT4, as seen in the corresponding ratio figures being greater than 1. Figure 11a shows that the greatest ratio of FLUKA to GEANT4 occurs at a value of 1.204 ± 0.004 at depth 1270 ± 10 mm, while Figure 11b shows this at a ratio of 1.66 ± 0.20 at depth 2710 ± 10 mm. Inspecting Figure 11a further, it is surprising that 1.0 GeV incident neutrons for a threshold of 10 MeV is stopped by the absorber plates, as seen by the plateau occurring at a FLUKA inefficiency of 0.004360 ± 0.000021 at a depth of 3750 ± 10 mm. One would expect high energy neutrons to travel deeper into the detector than shown for both FLUKA and GEANT4. Consulting Figure 50 in [2], which is displayed in Appendix D, 1 GeV incident neutrons do plateau with very thick 50 mm ab-

sorber plates, while for 10 mm thick absorber plates lower inefficiencies are reached. Considering the 20 mm thickness used in this project, a plateau somewhere in between these results was expected.

The lower threshold seen in Figure 11b, achieves the required inefficiency at (1.6±0.4) x 10^{-6} at a depth of 3830±10 mm, but it is unclear if a plateau is also seen here, or if the data seen at greater depths is due to statistical reasons. The statistical component refers to the fact that in these histogram plots, the uncertainty associated with inefficiency entry is estimated by taking the square root of the number of entries and normalising by dividing by the total number of entries. At shallow depths of the histogram, at high inefficiency, there are about 10 million entries and the corresponding uncertainty is quite small. At greater depths, there are a fewer entries and a larger uncertainty, as seen by the more visible error bars at greater depths. Therefore, one cannot speculate anything meaningful about the difference between the two simulation tools in the regions of greatest depth. Further inquiry into 1.0 GeV incident neutron energy and 1 MeV threshold would hence be of interest by simulating a greater number of events at greater depths and recreating the specific shower of an event in GEANT4. Investigation with divergent absorber widths would also prove constructive and if this identifies any further differences between the two simulation tools.

Figure 12a, with 3.0 GeV neutrons and a 10 MeV threshold, shows the FLUKA inefficiency of (1.2±0.35) x 10^{-6} at a depth of 3710±10 mm. Figure 12b, with 3.0 GeV neutrons and a 10 MeV threshold, shows the FLUKA inefficiency of (1.10±0.33) x 10^{-6} at a depth of 3150±10 mm. The greatest ratio out of all incident neutron energy also occurs here, with a value of 2.7±1.8, corresponding to depth 3390±10 mm. [2] estimates that a depth of ∼3 m is required for an inefficiency of 10^{-6}, which is similarly seen in Figure 12b, while Figure 12a seems to require a slightly greater depth. However, the inefficiency values at a greater depths produced in this study should not be treated as accurate quantitative results, due to the aforementioned statistical reasons. Instead, it may provide a qualitative overview of the approximate depth for the HCal veto inefficiency requirements. A more precise estimate of depth can be achieved by simulating a greater number of events, as well as more detailed bin sizes to accurately predict the position of energy deposition. Moreover, a primary limitation in this project relates to the geometry. As mentioned, previous study by [2] defined the HCal veto in terms of photo-electrons per scintillator bar, and also had different absorber thickness. Therefore, a direct comparison cannot be made of the estimated depth achieved by this project and the depth found in [2] for an inefficiency of 10^{-6}. Nonetheless, while this study cannot directly be used for the LDMX HCal, it has demonstrated that previous conclusions drawn by using GEANT4 are valid with another Monte Carlo tool FLUKA.

It is also noteworthy that the two thresholds provide negligible effects to the difference between FLUKA and GEANT4. This was expected for higher incident energies, as a higher energy incident neutron would on average deposit more energy per layer in the HCal, and is thereby less sensitive to where the threshold is set. A greater sensitivity could be achieved if the threshold was set close in value to the average energy deposition per layer, so if the threshold in this project had been increased, then greater differences for higher energy neutrons would be expected. This would imply that greater differences appear between thresholds for lower energy neutrons, which is seen in Figure 15 in Appendix C.

Sources of error that may have influenced the results of this project include the materials used to model the detector in FLUKA, displayed in Figure 13c and 13d in Appendix A, compared to GEANT4, as even slight differences in material composition could influence the validity of direct one to one comparison. Other assumptions that were not taken into consideration by both simulations would have influenced neutron behaviour, such as interaction cross section differences. This is

why for instance parameters of Birks law were removed from the GEANT4 samples since the FLUKA simulation did not take it into account.

Future work can be divided into two fronts. Firstly, by improving on the method put forth by this project. As mentioned, this includes analysing simulations with a greater number of events and different detector depths, as well as specifically focusing on the side HCal in order to estimate the veto inefficiency requirement for lower energy neutrons. This is another rare but important PN background that relies on the HCal veto system, usually in conjugation with other veto handles due to other charged particles being produced in these PN backgrounds. Secondly, by expanding the comparison between GEANT4 and other competing Monte Carlo simulation tools, such as PHITS [14] and MCNP [15].

6 Conclusion

The purpose of this project was to investigate neutron veto inefficiency of the LDMX using FLUKA and perform a comparison analysis to previous results by GEANT4. This was done by modelling a simplified LDMX HCal and directing high energy neutrons towards it, and measuring the subsequent energy depositions. Interpreting the results led to the conclusion that there was no significant difference between the two simulation tools FLUKA and GEANT4. This indicates that the current design of the LDMX HCal with a depth of $\sim$3 m is sufficient so as to ensure the veto performance for the relevant photo-nuclear (PN) backgrounds [2]. Improvements and future work motivated by this project include studying different energies and absorber thickness over a greater number of events and bin sizes, further scrutiny into the side HCal in order to find the veto requirements of lower energy neutrons, or new studies using other competing detector tools.

References

[1] B. R. Martin and G. Shaw. *Particle physics*. Wiley, 2017.

[2] Torsten Åkesson et al. *Light dark matter experiment (LDMX)*. Aug. 2018. URL: https://arxiv.org/abs/1808.05219.

[3] S. Agostinelli et al. *Geant4-A Simulation Toolkit*. June 2003. URL: https://www.sciencedirect.com/science/article/pii/S0168900203013688.

[4] J. Allison et al. *Recent developments in GEANT4*. July 2016. URL: https://www.sciencedirect.com/science/article/pii/S0168900216306957.

[5] J. Allison et al. *Geant4 developments and applications*. 2006. URL: https://ieeexplore.ieee.org/document/1610988.

[6] *CERN accelerating science*. URL: https://fluka.cern/.

[7] *CERN accelerating science*. URL: https://fluka.cern/documentation/examples/flair.

[8] Asher Berlin et al. *Dark matter, millicharges, Axion and scalar particles, gauge bosons, and other new physics with LDMX*. Oct. 2020. URL: https://arxiv.org/abs/1807.01730.

[9] Giles Barr et al. *Particle physics in the LHC era*. Oxford University Press, 2016.

[10] Marco Battaglieri et al. *US Cosmic Visions: New ideas in dark matter 2017: Community report*. July 2017. URL: https://arxiv.org/abs/1707.04591.

[11] Torsten Åkesson et al. *Current status and future prospects for the light dark matter experiment*. Mar. 2022. URL: https://arxiv.org/abs/2203.08192.

[12] Torsten Åkesson et al. *A high efficiency photon veto for the light dark matter experiment*. Dec. 2019. URL: https://arxiv.org/abs/1912.05535.

[13] William R. Leo. *Techniques for nuclear and particle physics experiments: A how-to approach*. 2nd ed. Springer, 1994.

[14] Jaea. *Phits homepage*. URL: https://phits.jaea.go.jp/.

[15] *The MCNP® code*. URL: https://mcnp.lanl.gov/.

Appendices

A. FLAIR Input File

The DEFAULT card was first set to CALORIME, making it suitable for calorimeter experiments. The BEAM was set to neutrons with energies in GeV and its direction specified to the positive z-direction in the BEAMPOS card. The four beam energies were set to 0.1 GeV, 0.5 GeV, 1.0 GeV and then 3.0 GeV.

A description of the problem geometry was added under the GEOBEGIN card. The first two spherical SPH cards denoted as void and blackbody represent the space surrounding the target and an all-absorbing region that avoids tracking particles to infinity, respectively. The HCal, as seen in Figure 6a, consists of 192 layers of alternating absorber and scintialltor boxes (no air in between), with 2 cm thickness so that the total detector has the dimensions of 200 cm x 200 cm x 384 cm. The steel absorbers and polystyrene scintillators were created using rectangular RPP cards, with each layer or "box" corresponding to a new REGION card. The materials stainless steel and polystyrene were created using MATERIAL and COMPOUND cards, and were then assigned to each region or layer using the ASSIGNMA card as seen in Figure 6b.

The estimator known as the EVENTBIN card was added, which was set to ASCII output and reproduces data with an energy deposition after each event, one step at a time. One event signifies one neutron directed to the HCal. The binning structure was set to 1x1x192, meaning that there are 192 bins in the z-direction, and one bin in the x- and y-directions. This allows for one energy deposition result in every steel and polystyrene layer.

At the end of the input file, the RANDOMIZ card was added which initialises different random sequences to distinguish histories. The number of events was specified to 100000 and later 10 million in the START card. A STOP card was added to indicate the end of the input data.

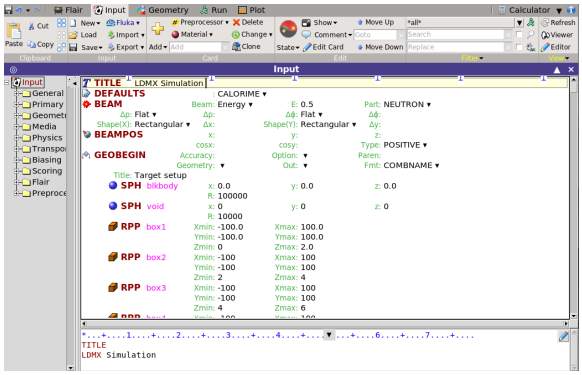

(a) The beam and body of the detector geometry.

(b) The detector region and the void and blackbody surrounding the detector.

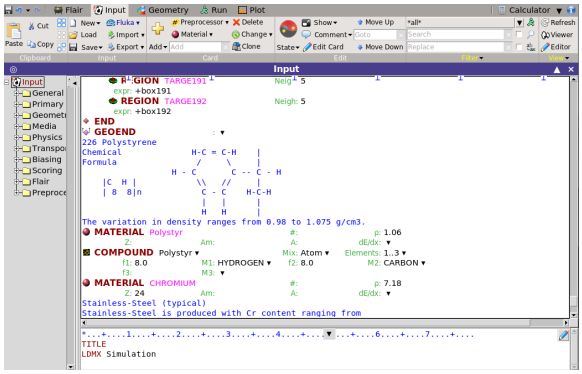

(c) The materials of the absorber and scintillator regions.

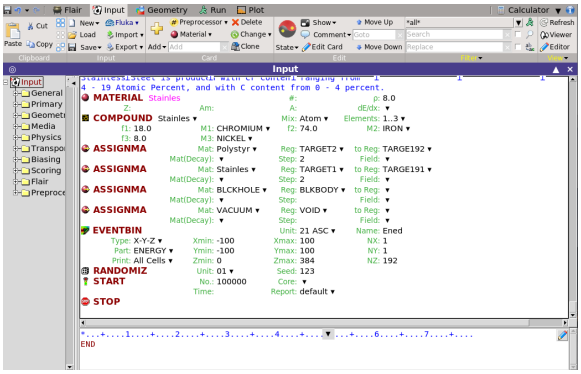

(d) The material assignment, scoring cards, start and stop cards.

Figure 13: FLAIR input.

B. Python Code

The following code was used to find the total energy absorbed by the steel and scintillator layers, the position of greatest energy deposition, and the single neutron veto inefficiency seen in Figures 7-12.

```
#Total Energy Absorbed in Steel and Scintillator layers

#For FLUKA samples
filename = ''
analysis = read_eventbin_file(filename)

#For GEANT4 samples change analysis to example
#example = read_ldmxsw_dump(N=N, particle='neutron', energy='', layers=96, runs=[1], use_birks=False)

num_events = analysis.num_events
energy_in_scintillator = np.zeros(num_events)
energy_in_steel = np.zeros(num_events)
Enedep = analysis.cards[0]
events = Enedep['events']
X = Enedep['X']
Y = Enedep['Y']
Z = Enedep['Z']
nx = X.num_bins
ny = Y.num_bins
nz = Z.num_bins
for ievent, event in enumerate(events):
    data = event.data
    for iz in range(nz):
        for iy in range(ny):
            for ix in range(nx):
                hit=data[ix][iy][iz]
                if iz % 2 == 0:
                    energy_in_steel[ievent] += hit
                else:
                    energy_in_scintillator[ievent] += hit


#Position of Greatest Energy Deposition

nre = analysis.num_events

maxAbsorbers = []
maxScintillators = []
zmaxAbsorbers = []
zmaxScintillators = []

first_card = analysis.cards[0]
events = first_card['events']
z = first_card['Z'].data

for i in range(nre):
    if i % (nre/100) == 0:
        print(f'{i / (nre / 100)} % ', end='')
```

```
    first_event = events[i]
    d = first_event.data[0][0]

    Absorbers = [d[j*2] for j in range(int(len(d)/2))]
    Scintillators = [d[j*2+1] for j in range(int(len(d)/2))]

    zAbsorbers = [z[j*2] for j in range(int(len(z)/2))]
    zScintillators = [z[j*2+1] for j in range(int(len(z)/2))]

    mAbsorbers = max(Absorbers)
    na = np.where(np.array(Absorbers)==mAbsorbers)[0][0]
    pAbsorbers = zAbsorbers[na]

    mScintillators = max(Scintillators)
    ns = np.where(np.array(Scintillators)==mScintillators)[0][0]
    pScintillators = zScintillators[ns]

    maxAbsorbers.append(mAbsorbers)
    maxScintillators.append(mScintillators)
    zmaxAbsorbers.append(pAbsorbers)
    zmaxScintillators.append(pScintillators)

Bins = list(z)
Bins = [0] + zScintillators
Bins.append(Bins[-1] + (Bins[-1] - Bins[-2])


#Inefficiency

def inefficiency(analysis, nre, threshold):
    tScintillators = []

    first_card = analysis.cards[0]
    events = first_card['events']
    z = first_card['Z'].data

    for i in range(nre):
        if i % (nre/100) == 0:
            print(f'{i / (nre / 100)} % ', end='')
        first_event = events[i]
        d = first_event.data[0][0]

        Scintillators = [d[j*2+1] for j in range(int(len(d)/2))]
        zScintillators = [z[j*2+1] for j in range(int(len(z)/2))]

        detect=False
        c=0
        for j in Scintillators:
            if j<threshold or detect:
                tScintillators.append(zScintillators[c])
            else:
                break
            c+=1

```

```
    Bins = list(z)
    Bins = [0] + zScintillators
    Bins.append(Bins[-1] + (Bins[-1] - Bins[-2])

    return tScintillators, Bins
```

C. Minimum Single Neutron Veto Inefficiency

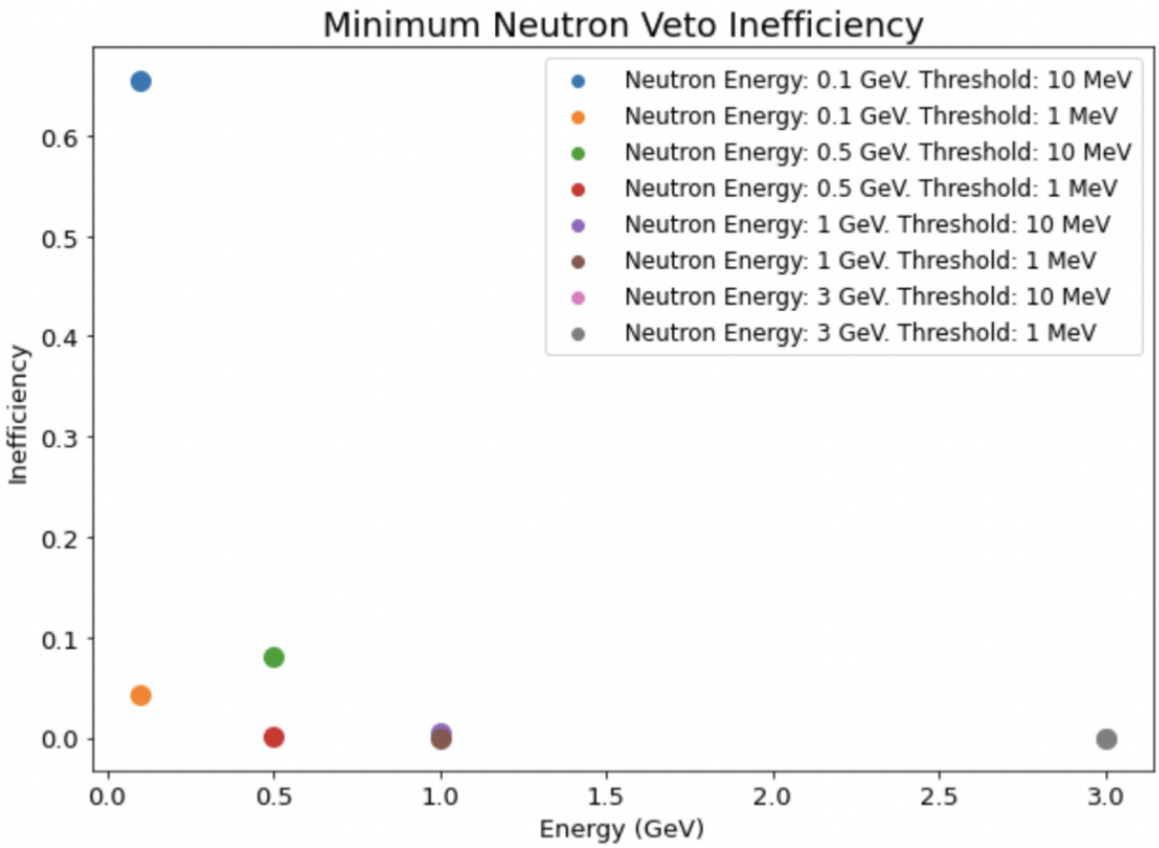

Figure 14: The minimum single neutron veto inefficiency achieved by the FLUKA samples. The plot shows this for 0.1 GeV, 0.5 GeV, 1.0 GeV and 3.0 GeV incident neutrons each with an energy threshold of 10 MeV and 1 MeV. The text displayed next to the data points shows the value of minimum inefficiency.

D. Single Neutron Veto Inefficiency from [2]

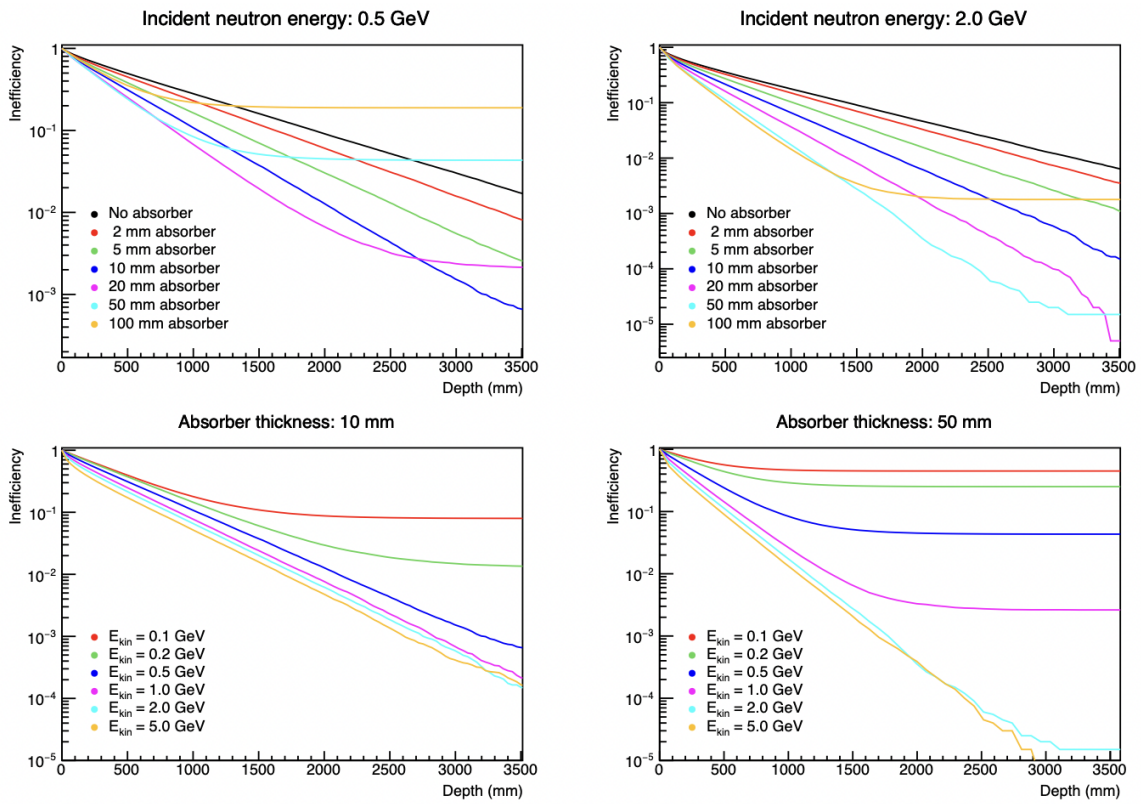

Figure 15: Figure 50 taken from page 67 of [2], which displays the single neutron veto inefficiency as a function of detector depth. Starting from the top left and continuing clockwise, plots for 500 MeV incident neutrons, 2 GeV incident neutrons, 10 mm absorber thickness and 50 mm absorber thickness are shown.